SUPPLEMENTARY INFORMATION

Understanding the structure-activity relationships of different double atom catalysts from density functional calculations: Three general rules for efficient CO oxidation

Qianyu Li[1,2], Junhui Zhou[1,2,3], Didi Li[1,2], Zhimin Ao[1,2]*

[1]*Guangdong-Hong Kong-Macao Joint Laboratory for Contaminants Exposure and Health, Guangzhou Key Laboratory Environmental Catalysis and Pollution Control, Institute of Environmental Health and Pollution Control, Guangdong University of Technology, Guangzhou 510006, China*
[2]*Guangdong Key Laboratory of Environmental Catalysis and Health Risk Control, Key Laboratory for City Cluster Environmental Safety and Green Development of the Ministry of Education, School of Environmental Science and Engineering, Guangdong University of Technology, Guangzhou 510006, PR China*
[3]*School of Environment, Beijing Normal University, Xinjiekouwai Street No. 19, Beijing 100875, PR China.*
Corresponding author's email address: zhimin.ao@gdut.edu.cn

Pages (15)

Tables (7)

- Table.S1 Geometrical and electronic parameters for UiO-66 and M/UiO-66.
- Table S2 The total energy of each structure corresponding to Fig. S5 above.
- Table. S3 The adsorption energy of atomic O on UiO-66 and M/UiO-66.
- Table. S4 The rate-limiting energy of barrier and the optimal mechanism of other reported DACs.
- Table. S5 The OC-O distance of IS, TS, and FS in the second CO oxidation of ER mechanism, and its corresponding energy of barrier.
- Table. S6 The energy barrier of each step in different mechanism, the d-band center (ε_d), the d-band center difference ($\Delta\varepsilon_d$), and the differential ratio ($\frac{\Delta\varepsilon_d}{\varepsilon_d(IS)}$) of IS and TS.
- Table. S7 The adsorption energy of each system for individual adsorbates and the corresponding rate-limiting E_{bar} under the optimal mechanism.

Figures (17)

- Fig. S1 The PDOS of each M/UiO-66.
- Fig. S2 The spin density of states of each M/UiO-66.
- Fig. S3 The frequency of each M/UiO-66.
- Fig. S4 The configuration of O_2 and CO adsorbed on M/UiO-66.
- Fig. S5 The PDOS of O_2 and CO molecule adsorbed on M/UiO-66.
- Fig. S6 The configuration of O_2 and CO adsorbed on Au, Cu, and Ag systems.
- Fig. S7 The top side of M/UiO-66 under ER, LH, and TER mechanism, and the situation of two CO molecules adsorbed.
- Fig. S8 The ER mechanism reaction pathway of Cd/UiO-66.
- Fig. S9 The ER mechanism reaction pathway of Cd/UiO-66 (another case).
- Fig. S10 The ER and LH mechanism reaction pathway of Pd/UiO-66.
- Fig. S11 The ER and LH mechanism reaction pathway of Cu/UiO-66.
- Fig. S12 The ER and LH mechanism reaction pathway of Ag/UiO-66.
- Fig. S13 The ER and LH mechanism reaction pathway of Au/UiO-66.
- Fig. S14 The TER mechanism reaction pathway of Cd/UiO-66.
- Fig. S15 The TER mechanism reaction pathway of Pt/UiO-66.
- Fig. S16 The TER mechanism reaction pathway of Cu/UiO-66.
- Fig. S17 The TER mechanism reaction pathway of Au/UiO-66.

Table S1 Geometrical parameters ($d_{\text{M-O}}$ and $d_{\text{M-M}}$) for the M/UiO-66, doping energies (E_b), Hirshfeld charge (Q), the d-band center (ε_d) and the upper-edge of the d band (ε_d^W) of the doped metal atom, respectively.

Metal	$d_{\text{M-O}}$ (Å)	$d_{\text{MA-MB}}$ (Å)	E_b (eV)	Q (e)	ε_d (eV)	ε_d^W (eV)
Ni	1.81	5.68	−11.49	0.08	-0.95	2.99
Pd	2.10	4.46	−6.98	0.31	-1.20	2.11
Pt	2.18	4.20	−6.39	0.18	-1.29	2.00
Cu	1.86	5.67	−10.57	0.26	-1.09	2.31
Ag	2.20	4.61	−8.16	0.36	-2.14	0.47
Au	2.28	4.37	−7.47	0.36	-2.37	0.25
Zn	1.80	5.84	−6.98	0.50	-8.38	-4.58
Cd	2.36	3.18	−7.57	0.34	-7.59	-5.19
Hg	2.43	3.10	−7.28	0.36	-6.99	-4.86

Table S2 The total energy of each structure corresponding to Fig. S5 above.

Structure	Total energy (Ha)
a2	-61193.65378
a4	-61193.65827
b2	-28736.12221
b4	-28736.11239
c2	-35854.56412
c4	-35854.55299

Table S3 The adsorption energy of atomic O on UiO-66 and M/UiO-66.

Group	System	E_{ads}(O) (eV)
/	UiO-66	-2.79
VIII	Pd/UiO-66	-1.50
	Pt/UiO-66	-1.60
IB	Cu/UiO-66	-0.34
	Ag/UiO-66	-0.54
	Au/UiO-66	-0.48
IIB	Zn/UiO-66	-3.14
	Cd/UiO-66	-1.78

Table S4 The rate-limiting energy of barrier (E_{bar}) and the optimal mechanism of other reported DACs.

Catalysts	Optimal mechanism	Rate-limiting E_{bar} (eV)	Reference
Zn/UiO-66 (Double atom catalyst, DAC)	Eley–Rideal (ER)	0.14	This research
Ag/UiO-66 (DAC)	termolecular ER (TER)	0.22	This research
Cd/UiO-66 (DAC)	ER	0.35	This research
Pd/UiO-66 (DAC)	TER	0.36	This research
Cu/UiO-66 (DAC)	ER	0.37	This research
Pt/UiO-66 (DAC)	ER	0.40	This research
Au/UiO-66 (DAC)	TER	0.58	This research
Cu_2@C_2N monolayer (DAC)	Langmuir–Hinshelwood (LH)	0.29	*Nanoscale*, 2018, **10**, 15696
Fe_1Cu_1@C_2N monolayer (DAC)	TER	0.42	*Small Methods*, 2019, **3**, 1800480
FeFe@N6 graphene (DAC)	TER	0.30	*Colloid Surf. A*,2021,**621**,126575
Au_1/Co_3O_4 (Single atom catalysts, SAC)	LH	0.14	*ACS Catal,* 2020, **10**, 6094−6101
Cu/V_b-BN (SAC)	TER	0.45	*Catal Today*, 2021,**368**, 148–160
Al-MoS_2 (SAC)	ER	0.19	*Appl. Surf. Sci*,2019,**484**,1297-1303
Ti/Zr_2CO_2 (SAC)	ER	0.58	*Appl. Surf. Sci*,2022,**575**,15177
MnO_2 (Metal Oxide)	Mars-van-Krevelen (Mvk)	0.54	*Appl. Catal. B*,2022, **300**, 120715
Au NPs/CeO2 (Nanoparticles, NPs)	Mvk	0.40	*ACS Catal*. 2018, **8**, 11491−11501

Table S5 The distance of OC-O of IS, TS, and FS in the oxidation process of the second CO under ER mechanism, and its corresponding energy of barrier (E_{bar}), the Cd-DAC has two situations*.

System	E_{bar}(eV)	*d*(OC-O) (Å)		
		IS	TS	FS
UiO-66	0.43	2.859	1.610	1.178
Pd/UiO-66	0.15	2.683	2.082	1.281
Pt/UiO-66	0.23	2.772	2.100	1.294
Cu/UiO-66	0.05	2.891	2.219	1.174
Ag/UiO-66	0.06	3.201	2.260	1.184
Au/UiO-66	0.07	2.817	2.090	1.183
Zn/UiO-66	0.14	2.996	2.037	1.179
Cd/UiO-66*	0.34	2.750	1.638	1.180
	0.94	1.306	1.276	1.173

***Text S1** The two situations of Cd-DAC are shown in Fig. S7 and S8.

Table S6 The energy barrier (E_{bar}) of each step in different mechanism, the d-band center (ε_d), the d-band center difference ($\Delta\varepsilon_d$) of the metal atom in IS and TS under all oxidation processes, and the corresponding differential ratio ($\frac{\Delta\varepsilon_d}{\varepsilon_d(IS)}$).

System	Mechanism-step	E_{bar} (eV)	ε_d (IS) (eV)	ε_d (TS) (eV)	$\Delta\varepsilon_d$ (eV)	$\frac{\Delta\varepsilon_d}{\varepsilon_d(IS)}$
Pd/UiO-66	ER-1	1.48	-1.77	-2.13	-0.36	20.34%
	ER-2	0.15	-2.20	-2.08	0.12	-5.45%
	LH-1	1.94	-1.87	-1.33	0.54	-28.88%
	TER-1	0.11	-2.24	-2.06	0.18	-8.04%
Pt/UiO-66	ER-1	0.40	-2.19	-1.63	0.56	-25.57%
	ER-2	0.23	-2.42	-2.14	0.28	-11.57%
	LH-1	1.74	-2.06	-2.66	-0.60	29.13%
	TER-1	0.80	-2.38	-2.29	0.09	-3.78%
Cu/UiO-66	ER-1	0.37	-2.10	-2.13	-0.03	1.43%
	ER-2	0.05	-1.82	-1.96	-0.14	7.69%
	LH-1	0.41	-2.48	-1.94	0.35	-14.11%
	TER-1	0.44	-2.33	-2.16	0.16	-6.87%
Ag/UiO-66	ER-1	0.84	-3.24	-2.80	0.44	-13.58%
	ER-2	0.06	-2.71	-2.87	-0.16	5.90%
	LH-1	1.00	-3.27	-2.86	0.41	-12.54%
	TER-1	0.22	-3.32	-3.42	-0.11	3.31%
Au/UiO-66	ER-1	1.05	-3.42	-3.09	0.33	-9.65%
	ER-2	0.07	-3.10	-3.09	0.01	-0.32%
	LH-1	2.05	-3.54	-3.30	0.24	-6.90%
	TER-1	0.58	-3.51	-3.16	0.36	-10.26%
Zn/UiO-66	ER-1	0.10	-6.29	-6.13	0.16	-2.54%
	ER-2	0.14	-5.53	-5.64	-0.11	1.99%
	TER-1	0.02	-5.15	-5.00	0.15	-2.91%
Cd/UiO-66	ER-1	0.13	-8.18	-7.77	0.41	-5.01%
	ER-2	0.34	-7.55	-8.44	-0.90	11.92%
	TER-1	0.46	-7.84	-8.17	-0.33	4.21%

Table S7 The adsorption energy of each system for individual adsorbates and the corresponding rate-limiting E_{bar} under the optimal mechanism.

System	Mechanism	E_{bar} (eV)	E_{ads} (O_2) (eV)	E_{ads} (CO) (eV)
UiO-66	ER	0.60	-0.82	-0.25
Pd/UiO-66	TER	0.35	-2.37	-2.03
Pt/UiO-66	ER	0.40	-2.48	-2.21
Cu/UiO-66	ER	0.36	-1.13	-1.27
Ag/UiO-66	TER	0.30	-0.49	-1.03
Au/UiO-66	TER	0.58	-0.32	-1.16
Zn/UiO-66	ER	0.10	-3.27	-0.95
Cd/UiO-66	ER	0.46	-1.49	-0.23

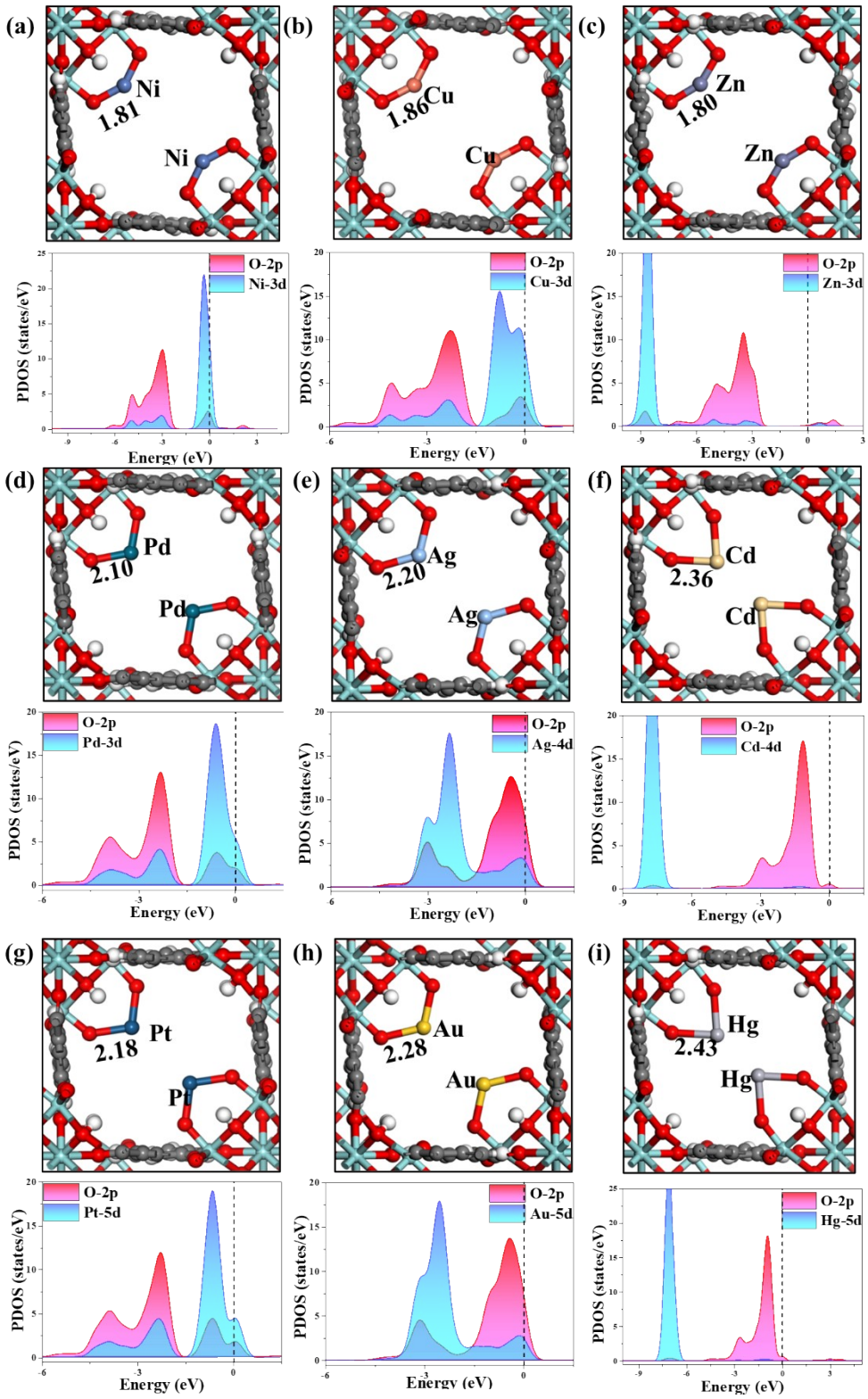

Fig. S1 In the PDOS of M/UiO-66, the intense hybridization suggests a strong interaction between the metal atom and substrate. The Fermi level is set to zero, as shown by the dashed line.

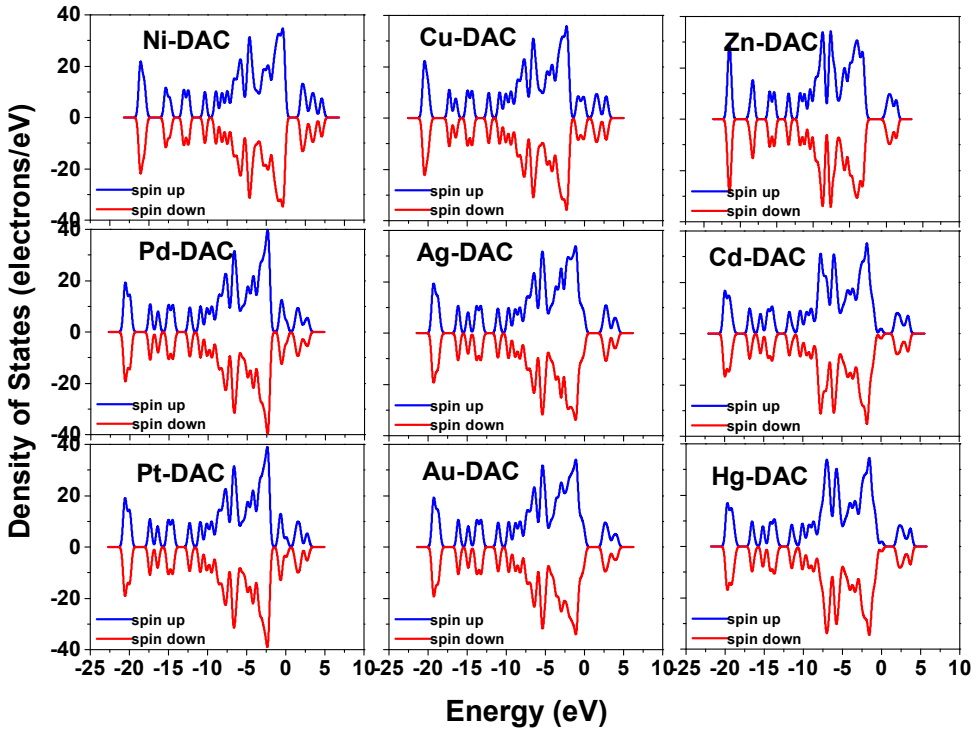

Fig. S2 The spin density of states of each M/UiO-66.

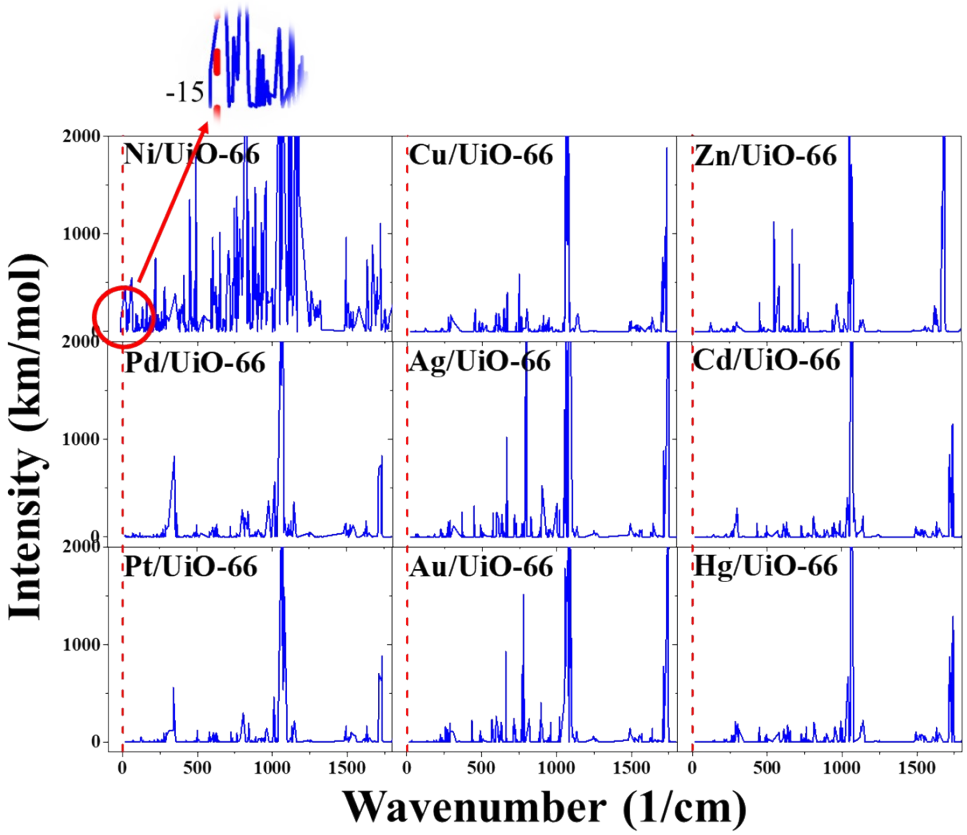

Fig. S3 The frequency of all M/UiO-66, the blue lines represent the frequency intensity at different wavelengths, and the dotted red lines represent the Fermi levels.

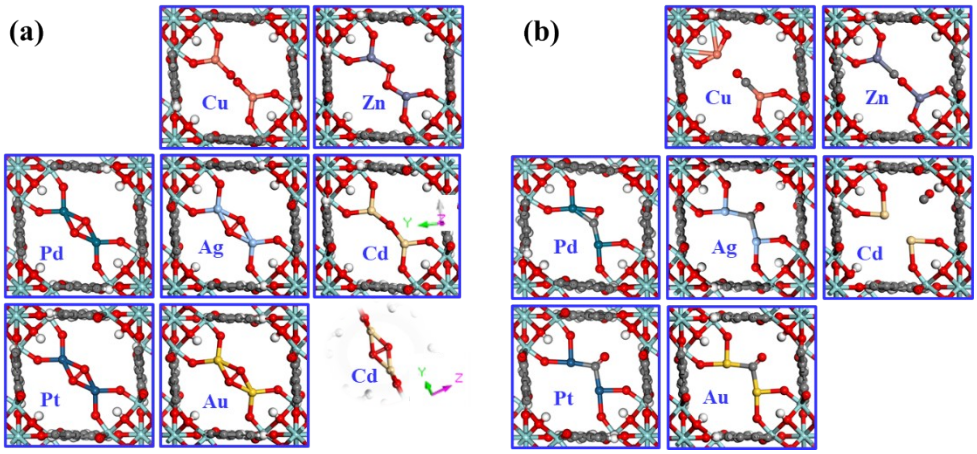

Fig. S4 The configuration of O_2 (a) and CO (b) adsorbed on M/UiO-66.

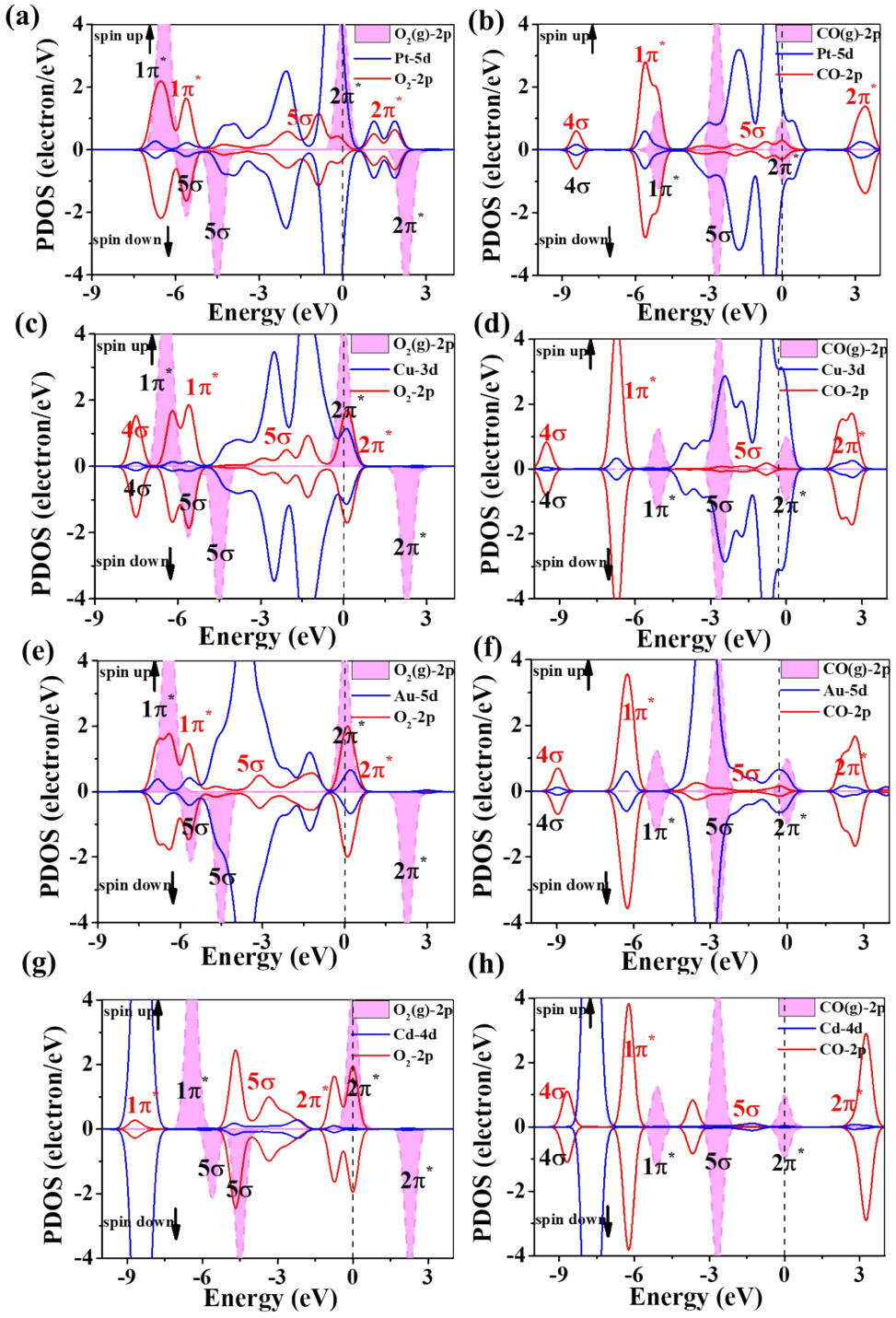

Fig. S5 The PDOS of O_2 and CO molecule adsorbed on M/UiO-66. The energy levels of the adsorbed O_2 and CO molecule orbitals are aligned according to the Fermi levels of the corresponding system. The Fermi level is set to zero, as shown by the dashed line.

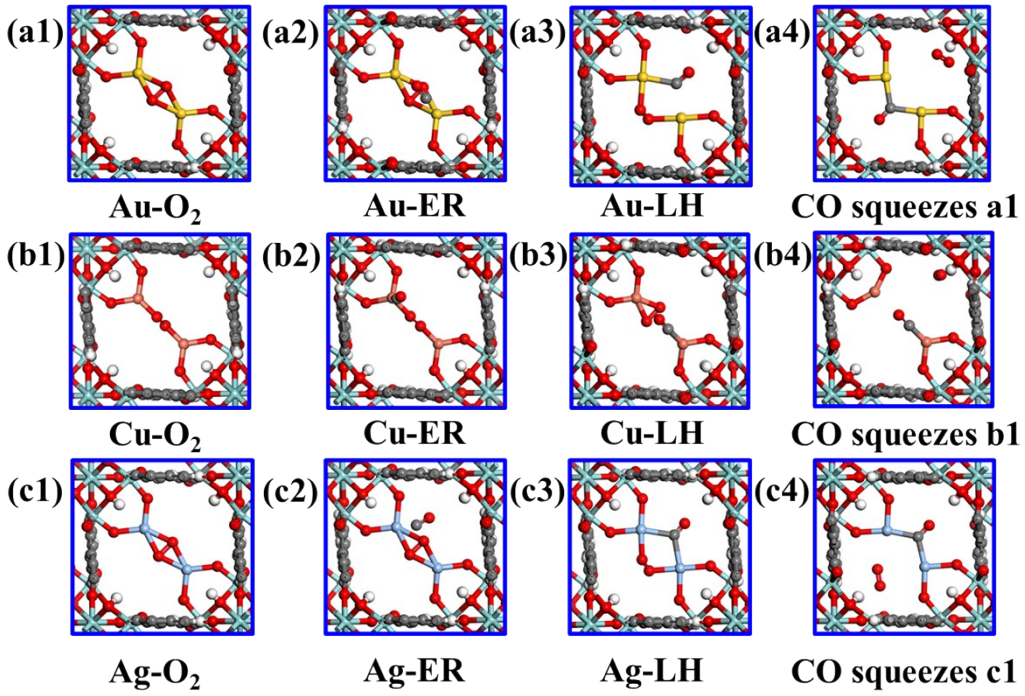

Fig. S6 The configuration of (a1, b1, and c1) O_2 molecule adsorbed and (a4, b4, and c4) CO molecule squeezes out O_2 molecule that has pre-adsorbed on Au, Cu, and Ag systems, the configuration under (a2, b2, and c2) ER and (a3, b3, and c3) LH mechanism of Au, Cu, and Ag-DACs.

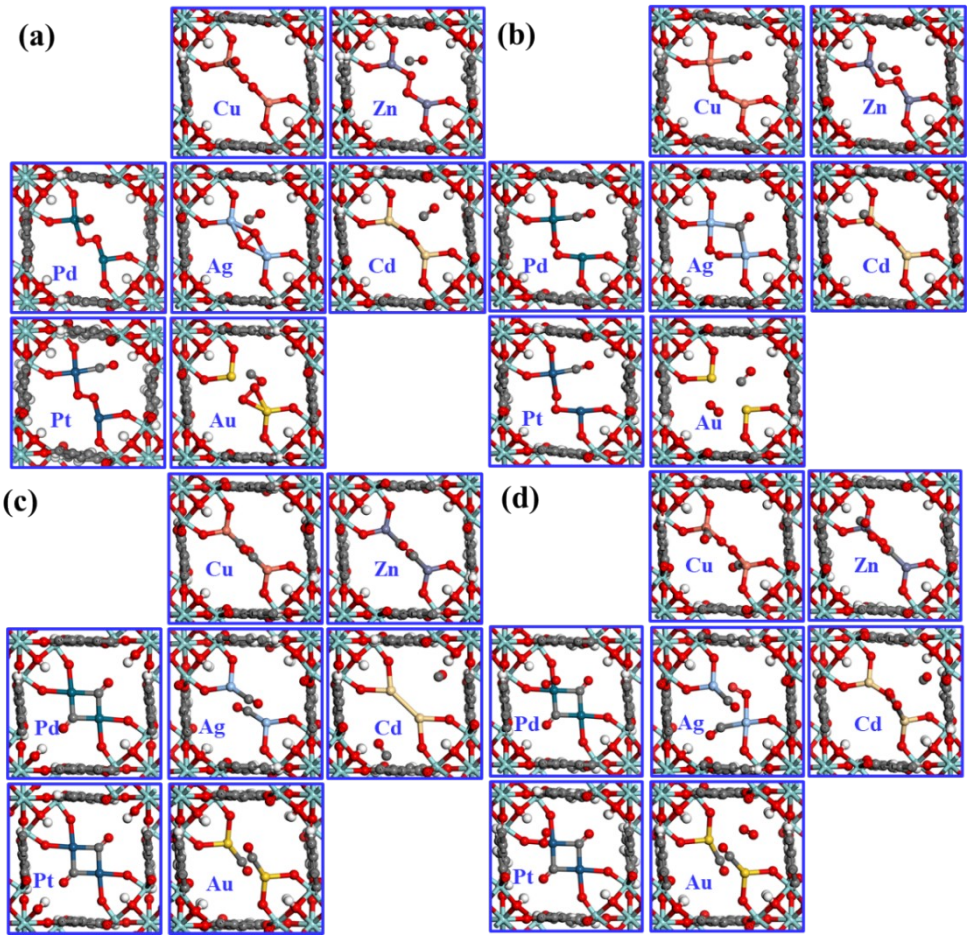

Fig. S7 The top side of M/UiO-66 under (a) ER mechanism, (b) LH mechanism, (c) two CO molecules adsorbed, and (d) TER mechanism.

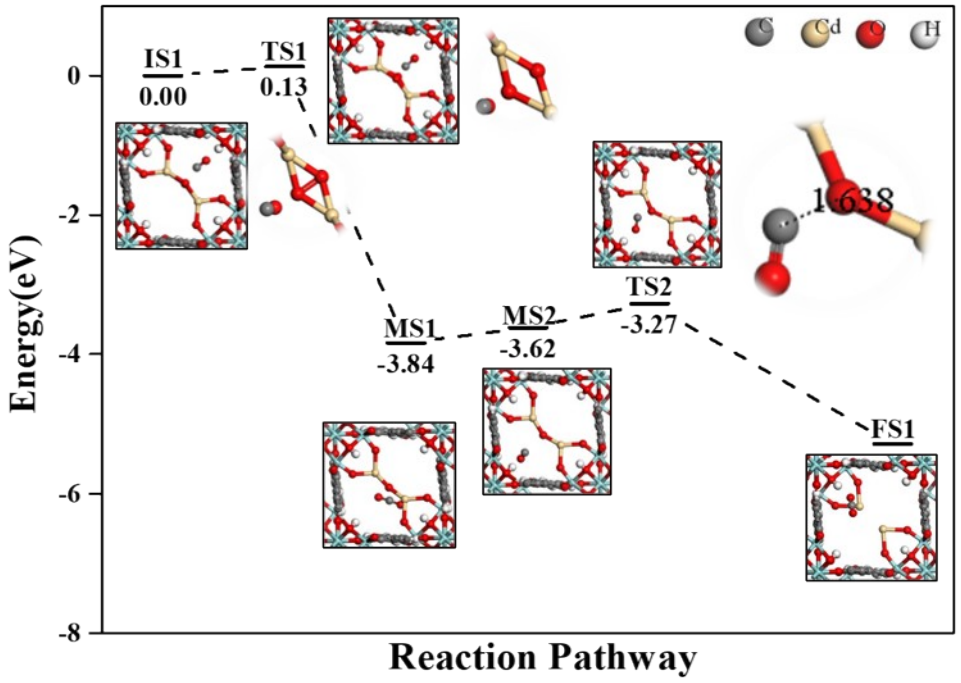

197

198 **Fig. S8** The ER mechanism reaction pathway of Cd/UiO-66 has two situations. This one is dominant, the other is
199 shown in Fig. S9.

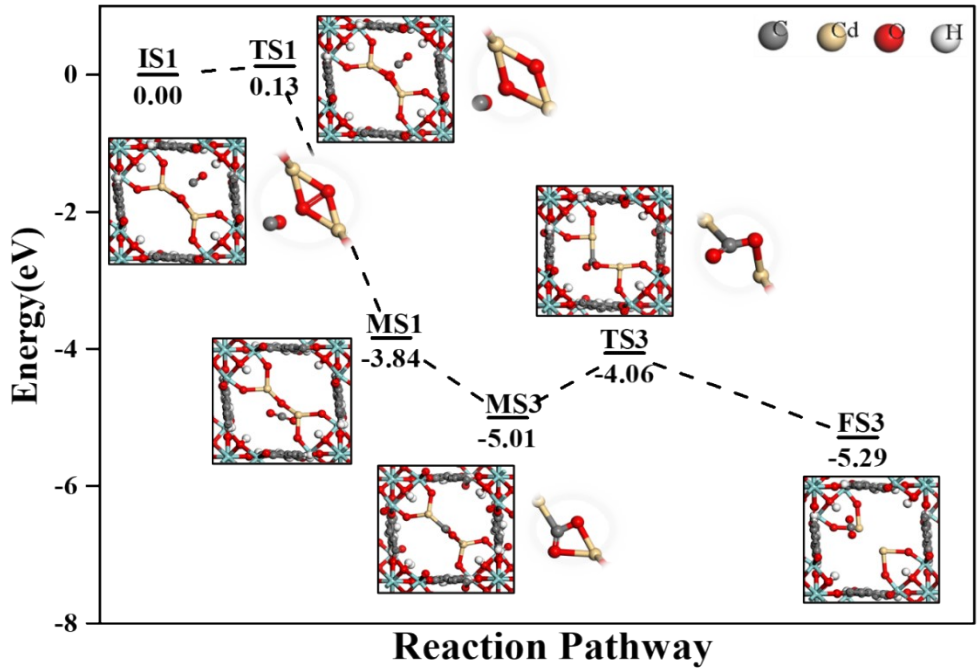

200 **Fig. S9** The ER mechanism reaction pathway of Cd/UiO-66 has two situations. This one is more vulnerable.

201
202
203
204
205
206
207
208

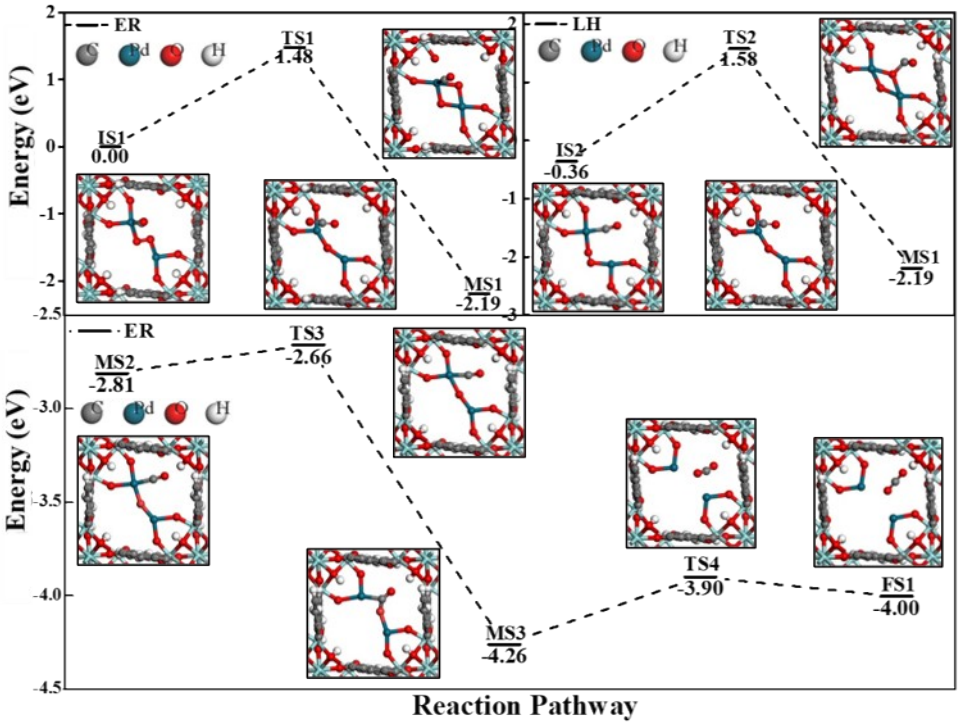

209 **Fig. S10** The ER and LH mechanism reaction pathway of Pd/UiO-66.

210

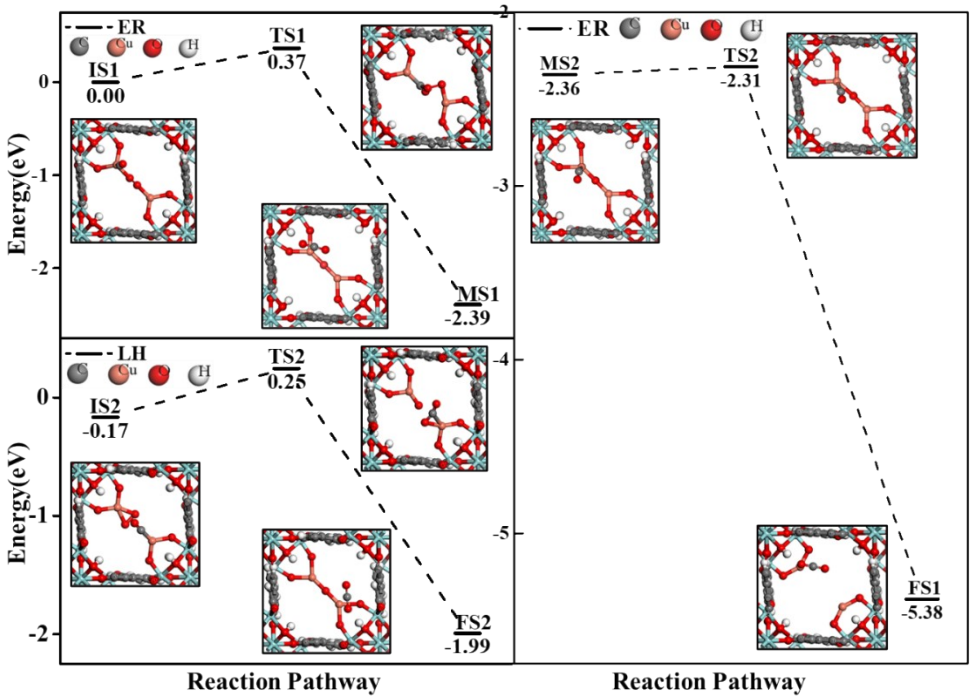

211

212 **Fig. S11** The ER and LH mechanism reaction pathway of Cu/UiO-66.

213
214
215
216
217

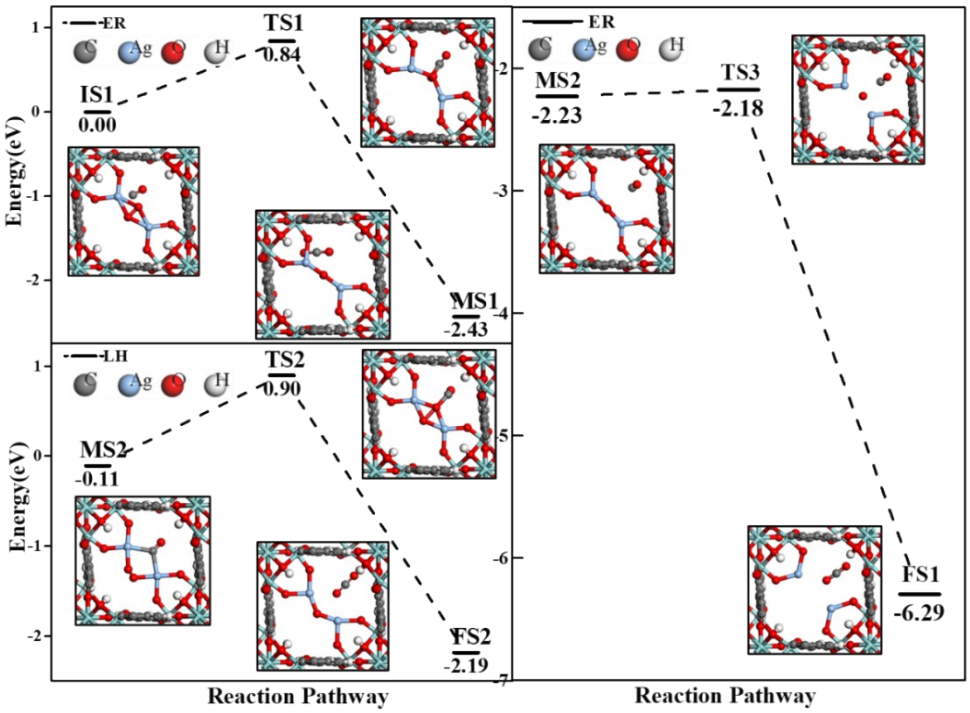

218
219
220

221 **Fig. S12** The ER and LH mechanism reaction pathway of Ag/UiO-66.

222

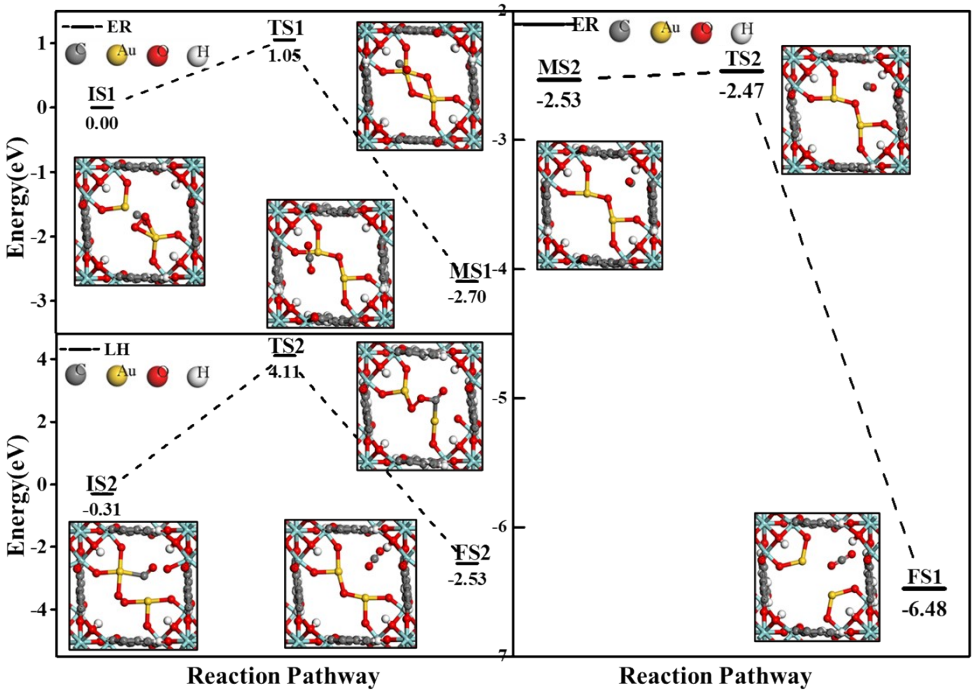

223
224

225 **Fig. S13** The ER and LH mechanism reaction pathway of Au/UiO-66.

226

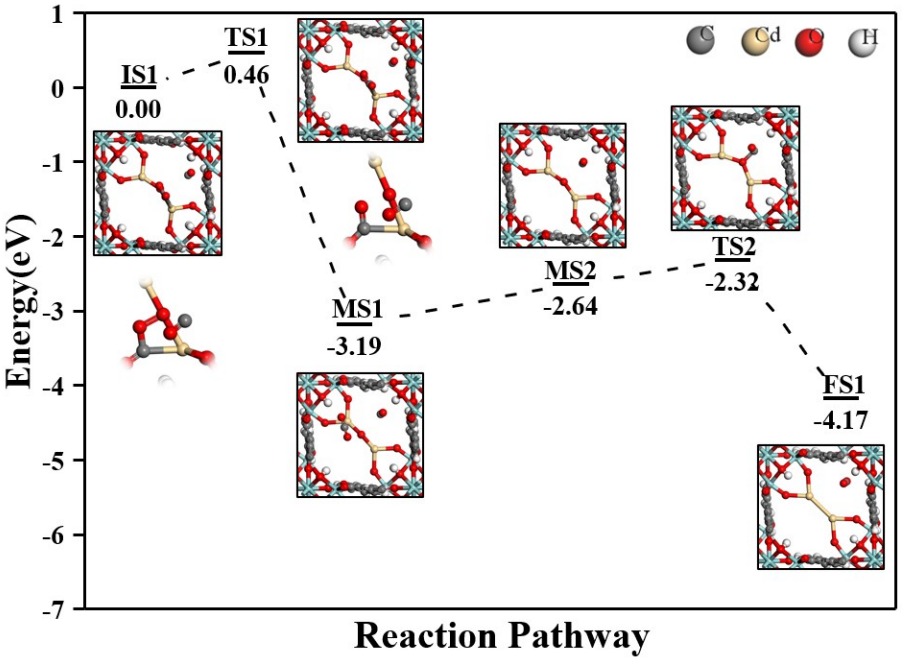

Fig. S14 The TER mechanism reaction pathway of Cd/UiO-66.

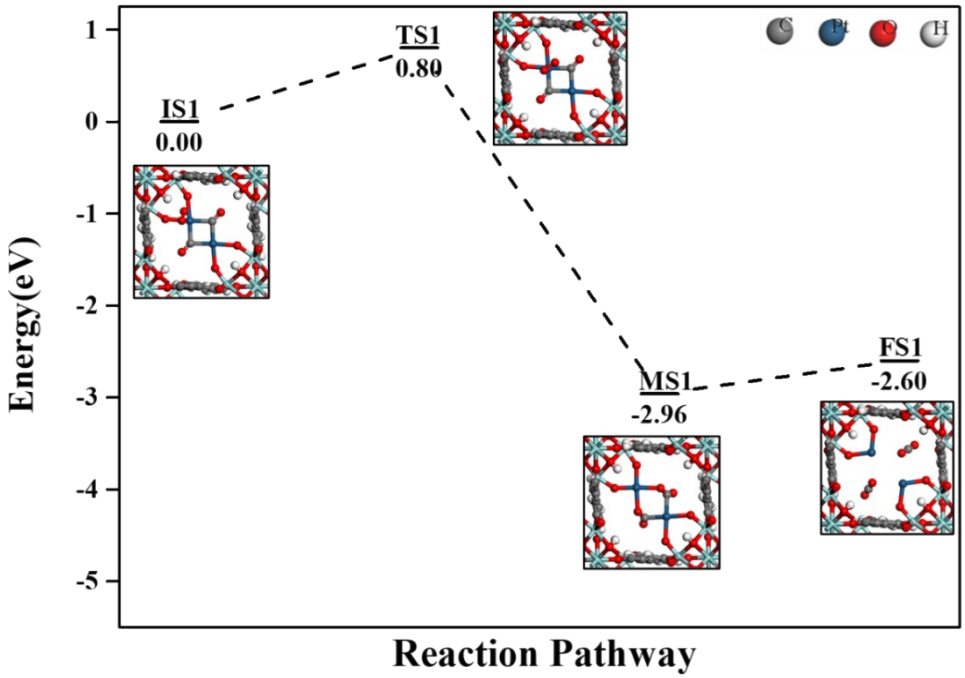

Fig. S15 The TER mechanism reaction pathway of Pt/UiO-66.

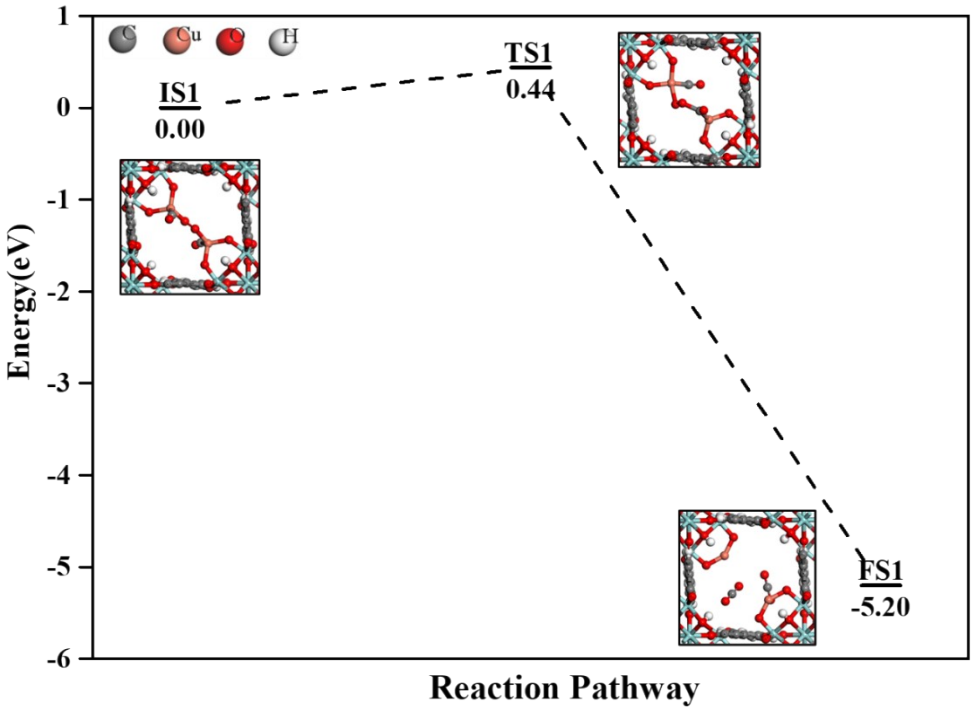

Fig. S16 The TER mechanism reaction pathway of Cu/UiO-66.

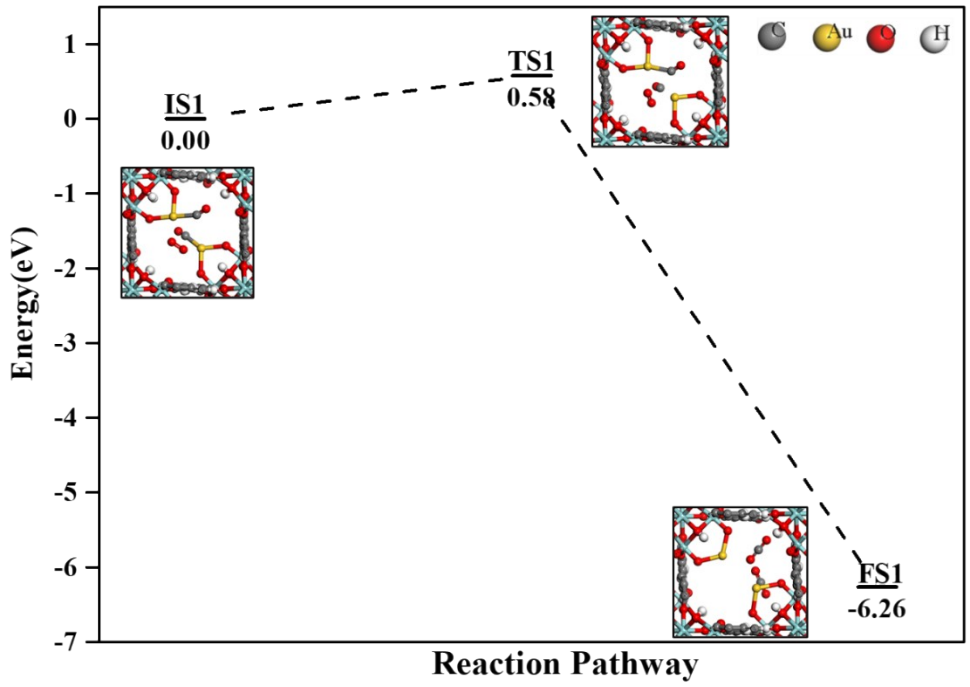

Fig. S17 The TER mechanism reaction pathway of Au/UiO-66.